Control of unstable steady states by extended time-delayed feedback

Thomas Dahms, Philipp Hövel, and Eckehard Schöll*
Institut für Theoretische Physik, Technische Universität Berlin, 10623 Berlin, Germany
(Received 27 July 2007; published 1 November 2007)

Time-delayed feedback methods can be used to control unstable periodic orbits as well as unstable steady states. We present an application of extended time delay autosynchronization introduced by Socolar *et al.* [Phys. Rev. E **50**, 3245 (1994)] to an unstable focus. This system represents a generic model of an unstable steady state which can be found, for instance, in Hopf bifurcation. In addition to the original controller design, we investigate effects of control loop latency and a bandpass filter on the domain of control. Furthermore, we consider coupling of the control force to the system via a rotational coupling matrix parametrized by a variable phase. We present an analysis of the domain of control and support our results by numerical calculations.

DOI: 10.1103/PhysRevE.76.056201 PACS number(s): 05.45.Gg, 02.30.Ks

I. INTRODUCTION

For over a decade, the stabilization of unstable and chaotic systems has been a field of extensive research. A variety of control schemes have been developed to control periodic orbits as well as steady states [1–3]. A simple and efficient scheme, introduced by Pyragas [4], is known as time delay autosynchronization (TDAS). This control method generates feedback from the difference of the current state of a system to its counterpart some time unit τ in the past. Thus, the control scheme does not rely on a reference system and has only a small number of control parameters, i.e., the feedback gain K and time delay τ. It has been shown that TDAS can stabilize both unstable periodic orbits, e.g., embedded in a strange attractor [4,5], and unstable steady states [6–8]. In the first case, TDAS is most efficient if τ corresponds to an integer multiple of the minimal period of the orbit. In the latter case, the method works best if the time delay is related to an intrinsic characteristic time scale given by the imaginary part of the system's eigenvalue [8]. A generalization of the original Pyragas scheme, suggested by Socolar, Sukow, and Gauthier [9], uses multiple time delays. This extended time delay autosynchronization (ETDAS) introduces a memory parameter R, which serves as a weight of states further in the past. A variety of analytic results about time-delayed feedback control are also known [10–13], for instance, in the case of long time delays [14] or the odd number limitation [15], which was refuted recently [16].

Although there has been a lot of research on the original Pyragas method [17,18], much less is known in the case of extended time-delayed feedback [19–24]. Recently it was shown that the additional memory parameter introduces a second time scale which leads to a strong improvement of the stabilization ability, for instance, arbitrary large correlations of stochastic oscillations without inducing a bifurcation [25].

In the present paper, we apply the ETDAS control method, which was initially invented to stabilize periodic orbits, to an unstable steady state realized as an unstable focus. This can be seen as a system close to but above a supercritical Hopf bifurcation. As a modification, we also consider an additional control loop latency, a bandpass filter, and different couplings.

This paper is organized as follows. In Sec. II, we introduce our model equations and develop the analytic tools used throughout the paper. Section III deals with a nondiagonal coupling implemented by a rotational matrix. In Sec. IV, we consider latency time effects, which arise if a time lag exists between calculation of the control force and reinjection into the system. Section V introduces a specific modification of ETDAS that includes a bandpass filtering of the control signal. This is important if high-frequency components are present in the system. Finally, we conclude with Sec. VI.

II. EXTENDED TIME-DELAYED FEEDBACK

We consider an unstable fixed point of focus type. Without loss of generality, the fixed point z^* is located at the origin. In complex center manifold coordinates z the linearized system can be written as $\dot{z}(t)=(\lambda+i\omega)z(t)$, where λ and ω are real numbers corresponding to the damping and oscillation frequency, respectively. The stability of the steady state is determined by the sign of the real part of the complex eigenvalue $\lambda+i\omega$. Since we consider an unstable focus, e.g., just above a Hopf bifurcation, we choose the parameter λ to be positive and ω nonzero. Separated in real and imaginary parts, i.e., $z(t)=x(t)+iy(t)$, the dynamics of the system is given by

$$\dot{\mathbf{x}}(t) = \mathbf{A}\mathbf{x}(t) - \mathbf{F}(t), \tag{1}$$

where $\mathbf{x}$ is the state vector composed of the real and imaginary part x and y of the variable z, the matrix $\mathbf{A}$ denotes the dynamics of the uncontrolled system

$$\mathbf{A} = \begin{pmatrix} \lambda & \omega \\ -\omega & \lambda \end{pmatrix}, \tag{2}$$

and $\mathbf{F}$ is the ETDAS control force, which can be written in three equivalent forms

$$\mathbf{F}(t) = K\sum_{n=0}^{\infty} R^n\{\mathbf{x}(t-n\tau) - \mathbf{x}[t-(n+1)\tau]\} \tag{3}$$

*schoell@physik.tu-berlin.de

$$= K[\mathbf{x}(t) - (1-R)\sum_{n=1}^{\infty} R^{n-1}\mathbf{x}(t-n\tau)] \quad (4)$$

$$= K[\mathbf{x}(t) - \mathbf{x}(t-\tau)] + R\mathbf{F}(t-\tau), \quad (5)$$

where K and τ denote the (real) feedback gain and time delay, respectively. $R \in (-1,1)$ is a memory parameter that takes into account those states that are delayed by more than one time interval τ. Note that $R=0$ yields the TDAS control scheme introduced by Pyragas [4].

The control force applied to the ith component of the system consists only of contributions of the same component. Thus, this realization is called diagonal coupling. We will consider a generalization to a nondiagonal coupling scheme in Sec. III. The first form of the control force [Eq. (3)] indicates the noninvasiveness of the ETDAS method because $\mathbf{x}^*(t-\tau)=\mathbf{x}^*(t)$ if the fixed point is stabilized. The third form [Eq. (5)] is best suited for an experimental implementation since it involves states further than τ in the past only recursively.

While the stability of the fixed point in the absence of control is given by the eigenvalues of matrix $\mathbf{A}$, i.e., $\lambda \pm i\omega$, one has to solve the following characteristic equation in the case of an ETDAS control force:

$$\Lambda + K\frac{1-e^{-\Lambda\tau}}{1-\mathrm{Re}^{-\Lambda\tau}} = \lambda \pm i\omega. \quad (6)$$

Due to the presence of the time delay τ, this characteristic equation becomes transcendental and possesses an infinite but countable set of complex solutions Λ. In the case of TDAS, i.e., $R=0$, the characteristic equation can be solved analytically in terms of the Lambert function [8,26–28]. We stress that for nonzero memory parameter R, however, such a compact analytic expression is not possible. Thus, one has to solve Eq. (6) numerically.

Figure 1 depicts the dependence of the largest real parts of the eigenvalue Λ upon the time delay τ according to Eq. (6) for different memory parameters R and fixed feedback gain $K=0.3$. The dashed, dotted, solid, dash-dotted, and dash-double-dotted curves (red, green, black, blue, and magenta) of $\mathrm{Re}(\Lambda)$ correspond to $R=-0.7$, -0.35, 0, 0.35, 0.7, respectively. The parameters of the unstable focus are chosen as $\lambda=0.1$ and $\omega=\pi$. Note that the time delay τ is given in units of the intrinsic period $T_0=2\pi/\omega$. When no control is applied to the system, i.e., $\tau=0$, all curves start at λ which corresponds to the real part of the uncontrolled eigenvalue. For increasing time delay, the real part of Λ decreases and eventually changes sign. Thus, the fixed point becomes stable. Note that there is a minimum of $\mathrm{Re}(\Lambda)$ indicating strongest stability if the time delay τ is equal to half the intrinsic period. For larger values of τ, the real part increases and becomes positive again. Hence, the system loses its stability. Above $\tau=T_0$, the cycle is repeated but the minimum of $\mathrm{Re}(\Lambda)$ is not so deep. The control method is less effective because the system has already evolved further away from the fixed point. For vanishing memory parameter $R=0$ (TDAS), the minimum is deepest, however, the control interval, i.e., values of τ with negative real parts of Λ, increases for larger R. Therefore the ETDAS control method is superior in comparison to the Pyragas scheme.

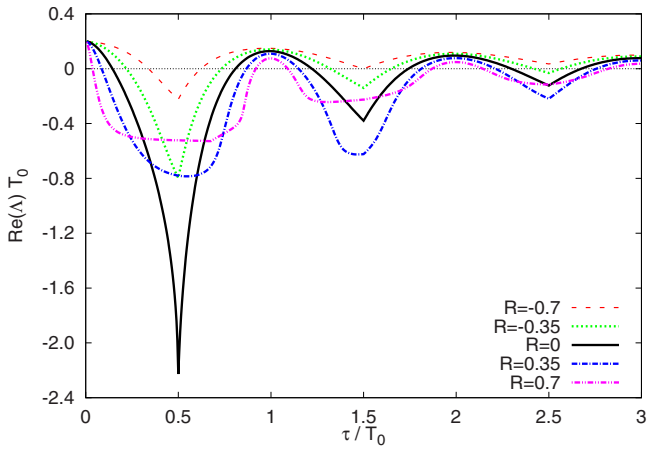

FIG. 1. (Color online) Largest real part of the complex eigenvalues Λ as a function of τ for different values of R. The dashed, dotted, solid, dash-dotted, and dash-double-dotted curves (red, green, black, blue, and magenta) correspond to $R=-0.7$, -0.35, 0, 0.35, 0.7, respectively. The parameters of the unstable focus are chosen as $\lambda=0.1$ and $\omega=\pi$ which yields an intrinsic period $T_0=2\pi/\omega=2$. The feedback gain K is fixed at $KT_0=0.6$.

Figure 2 shows the domain of control in the plane parametrized by the feedback gain K and time delay τ for different values of $R: 0, 0.35, 0.7, -0.35$ in Figs. 2(a)–2(d), respectively. The grayscale (color code) indicates only negative values of the largest real parts of the complex eigenvalue Λ. Therefore, Fig. 1 can be understood as a vertical cut through Fig. 2 for a fixed value of $KT_0=0.6$. Each panel displays several islands of stability which shrink for larger time delays τ. Note that no stabilization is possible if τ is equal to an integer multiple of the intrinsic period T_0. The domains of control become larger if the memory parameter R is closer to 1.

In order to obtain some analytic information of the domain of control, it is helpful to separate the characteristic

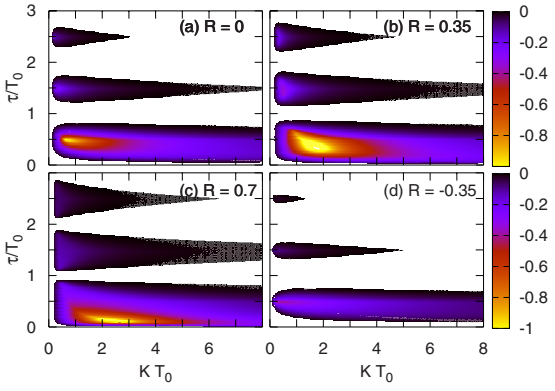

FIG. 2. (Color online) Domain of control in the (K,τ) plane for different values of $R: 0, 0.35, 0.7, -0.35$ in panels (a), (b), (c), and (d), respectively. The grayscale (color code) shows only negative values of the largest real part of the complex eigenvalues Λ according to Eq. (6). The parameters of the system are as in Fig. 1.

Eq. (6) into real and imaginary parts. This yields using $\Lambda = p + iq$

$$K(1 - e^{-p\tau}\cos q\tau) = \lambda - p - \mathrm{Re}^{-p\tau} \times [(\lambda - p)\cos q\tau \pm (\omega - q)\sin q\tau] \tag{7}$$

and

$$Ke^{-p\tau}\sin q\tau = \pm(\omega - q) + \mathrm{Re}^{-p\tau} \times [(\lambda - p)\sin q\tau \pm (\omega - q)\cos q\tau]. \tag{8}$$

The boundary of the domain of control is determined by a vanishing real part of Λ, i.e., $p=0$. With this constraint, Eqs. (7) and (8) can be rewritten as

$$K(1 - \cos q\tau) = \lambda - R[\lambda \cos q\tau \pm (\omega - q)\sin q\tau],$$

$$K \sin q\tau = \pm(\omega - q) + R[\lambda \sin q\tau \pm (\omega - q)\cos q\tau]. \tag{9}$$

At the threshold of control ($p=0, q=\omega$), there is a certain value of the time delay, which will serve as a reference in the following section, given by

$$\tau = \frac{(2n+1)\pi}{\omega} = \left(n + \frac{1}{2}\right)T_0, \tag{10}$$

where n is any non-negative integer. For this special choice of the time delay, the range of possible feedback gains K in the domain of control becomes largest as can be seen in Fig. 2. Hence, we will refer to this τ value as optimal time delay in the following. The minimum feedback gain at this τ can be obtained:

$$K_{\min}(R) = \frac{\lambda(1+R)}{2}. \tag{11}$$

Extracting an expression for $\sin(q\tau)$ from Eq. (9) and inserting it into the equation for the imaginary part leads after some algebraic manipulation to a general dependence of K on the imaginary part q of Λ

$$K(q) = \frac{(1+R)[\lambda^2 + (\omega - q)^2]}{2\lambda}. \tag{12}$$

Taking into account the multivalued properties of the arcsine function, this yields in turn analytical expressions of the time delay in dependence on q

$$\tau_1(q) = \frac{\arcsin\left(\frac{2\lambda(1-R^2)(\omega-q)}{\lambda^2(1-R^2)^2+(\omega-q)^2(1+R)^2}\right) + 2n\pi}{q},$$

$$\tau_2(q) = \frac{-\arcsin\left(\frac{2\lambda(1-R^2)(\omega-q)}{\lambda^2(1-R^2)^2+(\omega-q)^2(1+R)^2}\right) + (2n+1)\pi}{q}, \tag{13}$$

where n is a non-negative integer. Together with Eq. (12), these formulas describe the boundary of the domain of control in Fig. 2. Note that two expressions τ_1 and τ_2 are necessary to capture the complete boundary. The case of TDAS control was analyzed in Ref. [14] and is included as special choice of $R=0$.

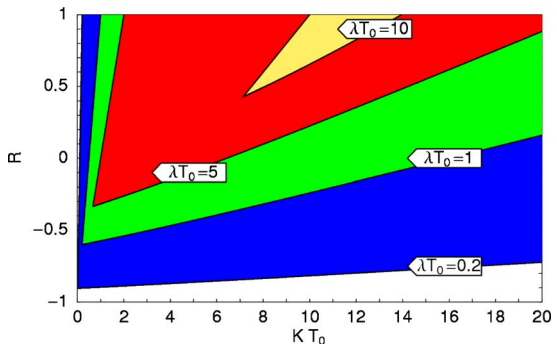

FIG. 3. (Color online) Domain of control in the (K,R) plane for different values of λ. The black, medium gray, dark gray, and light gray domains (blue, green, red, and yellow) correspond to $\lambda T_0 = 0.2$, 1, 5, and 10, respectively, as indicated. The time delay is chosen as $\tau = T_0/2$ and $\omega = \pi$.

For a better understanding of effects due to the memory parameter R, it is instructive to consider the domain of control in the plane parametrized by R and the feedback gain K. The results can be seen in Fig. 3, where the black, medium gray, dark gray, and light gray areas (blue, green, red, and yellow) correspond to the domain of control for $\lambda T_0 = 0.2$, 1, 5, and 10, respectively. The other system parameter is chosen as $\omega = \pi$. We keep the time delay constant at $\tau = T_0/2$. Note that the K interval for successful control increases for larger values of R. In fact, while the original Pyragas scheme, i.e., $R=0$, fails for $\lambda T_0 = 10$, the ETDAS method is still able to stabilize the fixed point. The upper left boundary corresponds to Eq. (11). The lower right boundary can be described by a parametric representation which can be derived from the characteristic Eq. (6):

$$R = \frac{\lambda\tau - \vartheta\tan(\vartheta/2)}{\lambda\tau + \vartheta\tan(\vartheta/2)}, \tag{14}$$

$$K\tau = \frac{\vartheta^2 + (\lambda\tau)^2}{\lambda\tau + \vartheta\tan(\vartheta/2)}, \tag{15}$$

where we used the abbreviation $\vartheta = (q-\omega)\tau$ for notational convenience. The range of ϑ is given by $\vartheta \in [0, \pi)$. A linear approximation leads to an analytic dependence of R and the feedback gain K given by a function $R(K)$ instead of the parametric Eqs. (14) and (15). A Taylor expansion around $\vartheta = \pi$ yields

$$K_{\max}(R) = \frac{\lambda^2 + \pi^2}{2\lambda}(R+1) + 2(R-1). \tag{16}$$

Another representation of the superior control ability of ETDAS is depicted in Fig. 4. The domain of control is given in the (K,λ) plane for different values of R. The light gray, dark gray, medium gray, and black areas (yellow, red, green, and blue) refer to $R=-0.35$, 0 (TDAS), 0.35, and 0.7, respectively. The time delay is chosen as $\tau = T_0/2$. One can see that for increasing R, the ETDAS method can stabilize systems in a larger λ range. However, the corresponding K interval for successful control can become small. See, for instance, the

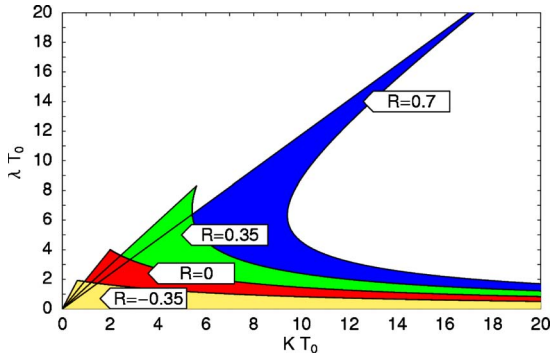

FIG. 4. (Color online) Domain of control in the (K,λ) plane for different memory parameters R. The light gray, dark gray, medium gray, and black domains (yellow, red, green, and blue) areas correspond to $R=-0.35$, 0 (TDAS), 0.35, and 0.7, respectively. The time delay is fixed at $\tau=T_0/2$.

black (blue) area ($R=0.7$) for large λ. A similar behavior was found in the case of stabilization of an unstable periodic orbit by ETDAS [29]. We stress that, as in the case of periodic orbits, the boundaries of the shaded areas can be calculated analytically from the following expression:

$$K\tau = \frac{(1-R)\vartheta}{\tan(\vartheta/2)}\left[\left(\frac{1+R}{1-R}\right)^2 + \tan^2(\vartheta/2)\right], \tag{17}$$

$$\lambda\tau = \frac{\vartheta}{\tan(\vartheta/2)}\left(\frac{1+R}{1-R}\right), \tag{18}$$

where we used $\vartheta=(q-\omega)\tau$ with $\vartheta\in[0,\pi)$ as in Eqs. (14) and (15). The maximum value for λ, which can be stabilized, is given by the special case $\vartheta=0$:

$$\lambda_{\max}\tau = 2\frac{1+R}{1-R}. \tag{19}$$

In this section, we have focused our discussion to the ETDAS method in the simplest realization of diagonal coupling. In the following, we will investigate the effects of nondiagonal coupling introduced by a variable phase.

III. PHASE DEPENDENT COUPLING

Time-delayed feedback has been widely used in optical systems both to study the intrinsic dynamics and to control the stabilization of, for instance, a laser device [30–35]. In these systems, the optical phase is an additional degree of freedom. We consider this additional control parameter as a generalization of the ETDAS feedback scheme using a nondiagonal coupling as opposed to the diagonal coupling discussed in the previous section. This nondiagonal coupling is realized by introducing a coupling matrix containing a variable phase φ:

$$\begin{pmatrix}\dot{x}\\ \dot{y}\end{pmatrix} = \begin{pmatrix}\lambda & \omega\\ -\omega & \lambda\end{pmatrix}\begin{pmatrix}x\\ y\end{pmatrix} - \begin{pmatrix}\cos\varphi & -\sin\varphi\\ \sin\varphi & \cos\varphi\end{pmatrix}\mathbf{F}(t). \tag{20}$$

In optical systems such as semiconductor lasers with external optical feedback [36,37], this feedback phase can be seen as the phase of the electric field. Experimentally, this phase of the feedback can be varied by tuning an external Fabry-Perot cavity. It has also been demonstrated that the feedback phase plays an important role in the suppression of collective synchrony in a globally coupled oscillator network [38].

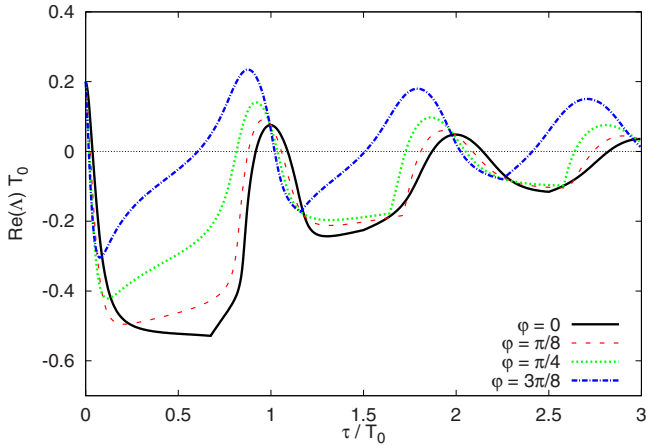

FIG. 5. (Color online) Largest real part of the eigenvalues Λ as a function of τ for different phases φ. The solid, dashed, dotted, and dash-dotted curves (black, red, green, and blue) correspond to $\varphi=0$, $\pi/8$, $\pi/4$, and $3\pi/8$, respectively. The other control parameters are fixed as $R=0.7$ and $KT_0=0.6$. The parameters of the system are as in Fig. 1.

The stability of the fixed point is again given by the largest real part of the complex eigenvalues Λ, which are calculated as the solutions of the following modified characteristic equation:

$$\Lambda + Ke^{\mp i\varphi}\frac{1-e^{-\Lambda\tau}}{1-\mathrm{Re}^{-\Lambda\tau}} = \lambda \pm i\omega. \tag{21}$$

Note that this equation differs from the characteristic equation in the diagonal case (see Sec. II) by an additional exponential term. This is due to the choice of phase-dependent coupling by a rotational matrix. We stress that a similar phase factor has recently been used [16] to overcome a topological limitation of time-delayed feedback control known as the "odd number limitation theorem," which refers to the case of an unstable periodic orbit with an odd number of real Floquet multipliers larger than unity [15,39].

In analogy to Sec. II a minimum feedback gain can be calculated:

$$K_{\min} = \frac{\lambda(1+R)}{2\cos\varphi}. \tag{22}$$

Note that the time delay that corresponds to this value of $K_{\min}$ is no longer given by Eq. (10) and is not the optimal time delay in the general case of nonzero phase. Nevertheless, Eq. (22) can be used as a coarse estimate of the minimum feedback gain for the regime of small values of φ, if the time delay is chosen as Eq. (10).

Figure 5 depicts the dependence of the largest real part of

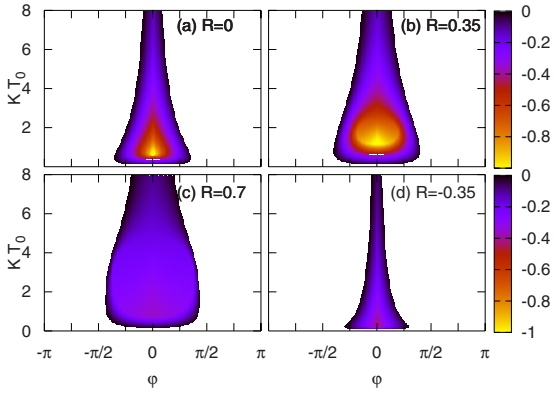

FIG. 6. (Color online) Domain of control in the (φ, K) plane for optimal time delay $\tau = T_0/2$. Panels (a), (b), (c), and (d) correspond to a memory parameter R of 0, 0.35, 0.7, and −0.35, respectively. The grayscale (color code) shows the largest real part of the complex eigenvalues Λ as given by Eq. (21). Only negative values are displayed. The parameters of the system are as in Fig. 1.

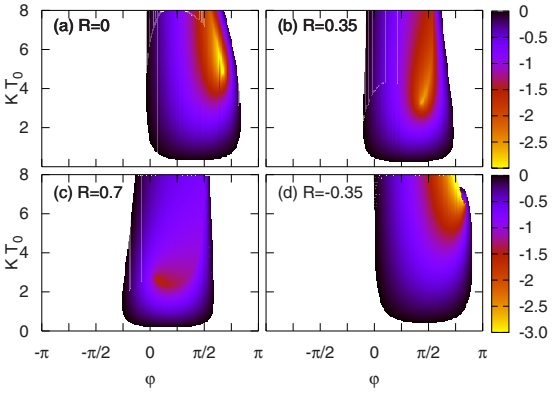

FIG. 7. (Color online) Domain of control in the (φ, K) plane for time delay $\tau = 0.1T_0$. Panels (a), (b), (c), and (d) correspond to a memory parameter R of 0, 0.35, 0.7, and −0.35, respectively. The grayscale (color code) shows the largest real part of the complex eigenvalues Λ as given by Eq. (21). Only negative values are depicted. The parameters of the system are as in Fig. 1.

the eigenvalues Λ on the time delay τ for fixed values of $R = 0.7$ and $KT_0 = 0.6$ but different values of the phase. The solid, dashed, dotted, and dash-dotted curves (black, red, green, and blue) correspond to $\varphi = 0$, $\pi/8$, $\pi/4$, and $3\pi/8$, respectively. It can be observed that the control is overall less effective for larger φ, as the curves are shifted up toward positive real parts for increasing the phase. The range of possible values for the time delay shrinks. The optimal time delay is shifted toward smaller values for larger φ, which can be seen for the case of $\varphi = 3\pi/8$, where the optimal time delay is in the range of $\tau = 0.1T_0$ instead of $0.5T_0$, which was the optimal time delay for $\varphi = 0$ according to Eq. (10).

The four-dimensional parameter space is now given by the feedback gain K, time delay τ, memory parameter R, and feedback phase φ. At first, we consider the domain of control in the plane parametrized by K and φ. Hence, we keep the other remaining control parameters R and τ fixed. Figures 6 and 7 show the domain of control for a time delay of $T_0/2$ and $0.1T_0$, respectively. In each figure, the memory parameter R is chosen as $R = 0$, 0.35, 0.7, and −0.35 in panels (a), (b), (c), and (d), respectively. The grayscale (color code) corresponds to the largest real part of the complex eigenvalues as calculated from Eq. (21). Only negative values are depicted, i.e., those combinations of K and φ for which the control scheme is successful. Note that the case $R = 0$ corresponds to the TDAS control method [37]. An increase of the memory parameter R leads to a larger domain of control. Even though the system can be stabilized for a larger range of K and φ, the system becomes less stable overall, since the real part of Λ is closer to zero. For negative values of R, the domain of control shrinks. Note that also in the case of nonoptimal time delay as in Fig. 7 the range of choice for possible feedback gain and phase is enlarged.

For a better understanding of the effects of the feedback phase, Fig. 8 depicts the domain of control in the (K, R) plane. The black, medium gray, dark gray, and light gray areas (blue, green, red, and yellow) correspond to successful control for $\varphi = 0$, $\pi/8$, $\pi/4$, and $3\pi/8$, respectively. Figure 8(a) shows the case of optimal time delay, i.e., $\tau = T_0/2$; Fig. 8(b) displays the case of $\tau = 0.1T_0$. Note that an increase of φ leads to a smaller domain of control in the case of $\tau = T_0/2$. This effect, however, is reversed for nonoptimal choices of τ, where the phase φ compensates for the bad choice of the time delay. Thus, control is possible again, for instance, in the TDAS case $(R = 0)$ for $\varphi = 3\pi/8$. Following the strategy introduced in Sec. II, one can also derive parametric formulas for the boundary of the domain of control in the case $\varphi \neq 0$:

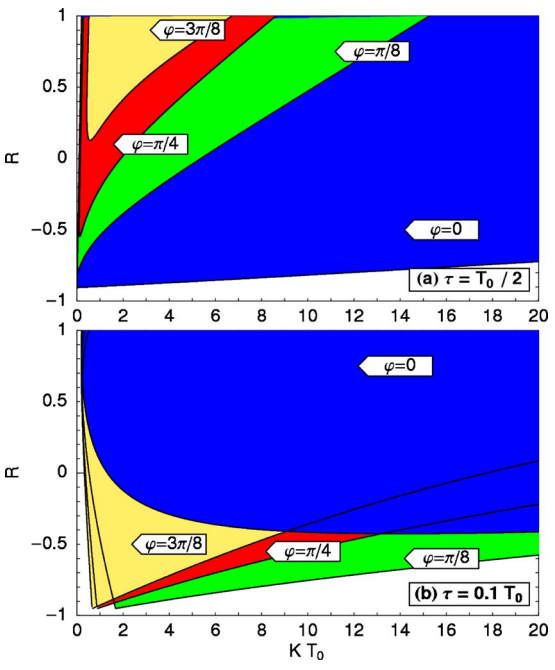

FIG. 8. (Color online) Domain of control in the (K, R) plane for different values of the feedback phase φ. The black, medium gray, dark gray, and light gray areas (blue, green, red, and yellow) correspond to $\varphi = 0$, $\pi/8$, $\pi/4$, and $3\pi/8$, respectively. Panel (a) displays the domain of control for optimal $\tau = T_0/2$ and panel (b) for $\tau = 0.1T_0$. The parameters of the system are as in Fig. 1.

$$R = \frac{\vartheta[\cos(\omega\tau + \vartheta + \varphi) - \cos\varphi] + \lambda\tau[\sin\varphi - \sin(\omega\tau + \vartheta + \varphi)]}{\vartheta[\cos\varphi - \cos(\omega\tau + \vartheta + \varphi)] - \lambda\tau[\sin\varphi + \sin(\omega\tau + \vartheta + \varphi)]}, \tag{23}$$

$$K\tau = \frac{(\vartheta^2 + \lambda^2\tau^2)\cos\left[\frac{1}{2}(\omega\tau + \vartheta)\right]}{\lambda\tau\cos\left[\frac{1}{2}(\omega\tau + \vartheta) - \varphi\right] - \vartheta\sin\left[\frac{1}{2}(\omega\tau + \vartheta) - \varphi\right]}. \tag{24}$$

We stress that it is possible to derive expression of $K(q)$ and $\tau(q)$ similar to Eqs. (12) and (17) also in the case of $\varphi \neq 0$. These calculations are lengthy and do not produce more insight and thus are omitted here.

IV. CONTROL LOOP LATENCY

After the investigation of nondiagonal coupling, we consider in this section an additional control loop latency. This latency is associated with time required for the generation of the control force and its reinjection into the system. In an optical realization, for instance, the latency time is given by the propagation time of the light between the laser and the Fabry-Perot control device. We stress that in the case of unstable periodic orbits, Just has shown that longer latency times reduce the control abilities of the time-delayed feedback of TDAS type [29]. Similar results were found for ETDAS [24].

The latency time δ acts as an additional time delay in all arguments of the control force of Eq. (3). Using the recursive form of $\mathbf{F}$ as given by Eq. (5), this yields

$$\mathbf{F}(t) = [\mathbf{x}(t-\delta) - \mathbf{x}(t-\delta-\tau)] + R\mathbf{F}(t-\tau). \tag{25}$$

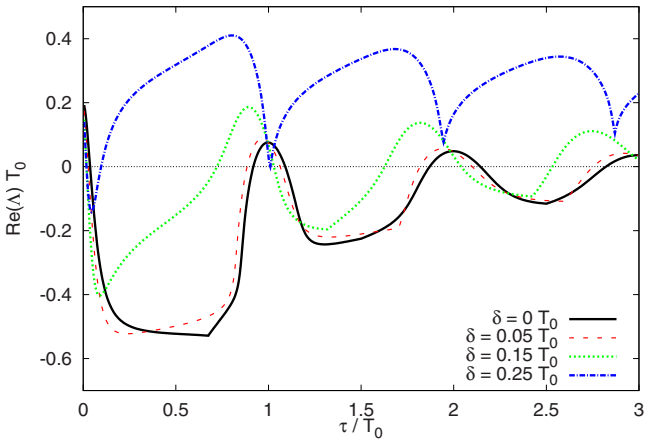

FIG. 9. (Color online) Largest real part of the eigenvalues Λ as a function of τ for different latency times δ. The solid, dashed, dotted, and dash-dotted curves (black, red, green, and blue) correspond to $\delta=0$, $0.05T_0$, $0.15T_0$, and $0.25T_0$, respectively. The other control parameters are fixed as $R=0.7$ and $KT_0=0.6$. The parameters of the system are as in Fig. 1.

The characteristic Eq. (6) is now modified by an additional exponential factor

$$\lambda \pm i\omega = \Lambda + Ke^{-\Lambda\delta}\frac{1 - e^{-\Lambda\tau}}{1 - \mathrm{Re}^{-\Lambda\tau}}. \tag{26}$$

In contrast to the previous section, this exponential term depends on the eigenvalue Λ itself.

Figure 9 depicts the dependence of the largest real part of the eigenvalues Λ on the time delay τ for fixed values of $R=0.7$ and $KT_0=0.6$, but different latency times. The solid, dashed, dotted, and dash-dotted curves (black, red, green, and blue) correspond to $\delta=0$, 0.1, 0.3, and 0.5, respectively. It can be seen that the control scheme is less successful for longer latency times. The τ interval with negative real parts of Λ becomes smaller. In the case of $\delta=0.25T_0$, for instance, control can only be achieved in a narrow range of small τ and the second minimum does not reach down to negative Re(Λ) anymore. In addition, the minima of the real parts are distorted and shifted toward smaller time delays.

Taking also a varying feedback gain K into account, the domain of control can be seen in Fig. 10. The other control parameters are fixed at $\tau=T_0/2$ and $R=0.7$. Figures 10(a)–10(d) correspond to values of $\delta=0$, 0.1τ, 0.2τ, and 0.3τ, respectively. As in Figs. 6 and 7 of the previous section, the grayscale (color code) corresponds to the largest real part of the complex eigenvalues which are calculated from

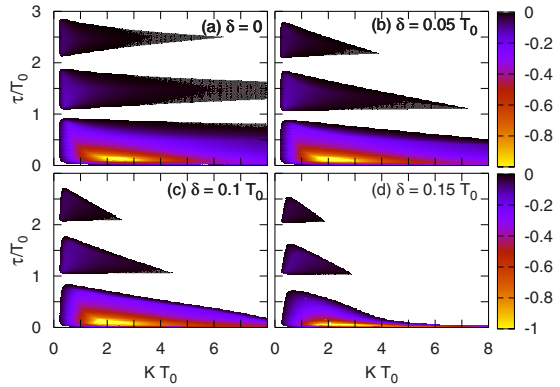

FIG. 10. (Color online) Domain of control in the (K,τ) plane for different values of the latency time δ and fixed $R=0.7$. Panels (a), (b), (c), and (d) correspond to values of $\delta=0$, $0.05T_0$, $0.1T_0$, and $0.15T_0$, respectively, where the time delay is fixed at $\tau=T_0/2$. The grayscale (color code) shows the largest real part of the complex eigenvalues Λ as given by Eq. (26). Only negative values are displayed. The parameters of the system are as in Fig. 1.

Eq. (26). Note that only negative values are depicted. For increasing latency time, the domains of control shrink. Similar to the discussion in the one-dimensional projection of Fig. 9, the islands are distorted toward smaller time delays.

Separating the characteristic Eq. (26) into real and imaginary part, one can derive, in analogy to Sec. II, an expression for the minimum feedback gain

$$K_{\min}(\delta) = \frac{\lambda(1+R)}{\cos[(2n+1)\pi\delta/\tau]}, \tag{27}$$

which is consistent with the TDAS case investigated in Ref. [8].

As another two-dimensional projection of the parameter space, Fig. 11 displays the domain of control in the (K,R) plane for different values of the latency time δ. The black, medium gray, dark gray, and light gray areas (blue, green, red, and yellow) refer to values of $\delta=0$, $0.05T_0$, $0.1T_0$, and $0.15T_0$, respectively. Similar to Fig. 8, Fig. 11(a) shows the case of optimal choice of the time delay $\tau=T_0/2$ and Fig. 11(b) refers to $\tau=T_0/8$. In the first case, the domain of control shrinks considerably for increasing δ, whereas in the latter case, this change is less pronounced.

Similar to the previous sections, it is possible to derive a parametric expression for the boundary of the domain of control [$R(\vartheta)$ and $K(\vartheta)$]:

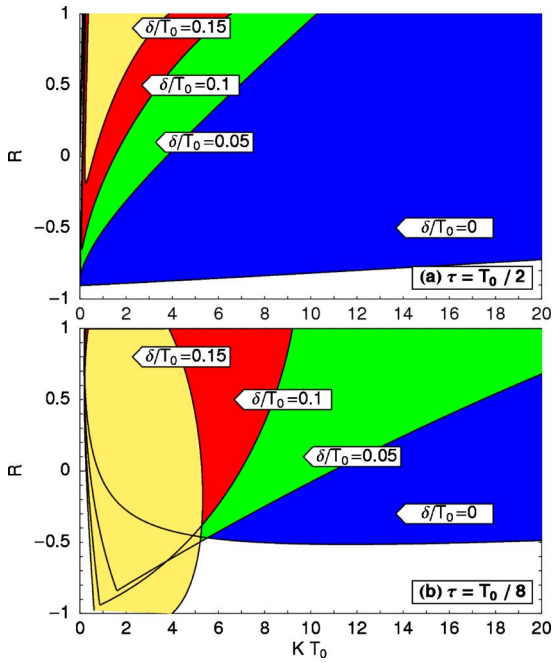

FIG. 11. (Color online) Domain of control in the (K,R) plane for different values of the latency time δ. The black, medium gray, dark gray, and light gray areas (blue, green, red, and yellow) refer to values of $\delta=0$, $0.05T_0$, $0.1T_0$, and $0.15T_0$, respectively. Panel (a) corresponds to an optimal time delay $\tau=T_0/2$ and panel (b) to $\tau=T_0/8$. The parameters of the system are as in Fig. 1.

$$R = \frac{-\vartheta\cos\left[(\omega\tau+\vartheta)\frac{\delta}{\tau}\right] + \vartheta\cos\left[(\omega\tau+\vartheta)\left(1+\frac{\delta}{\tau}\right)\right] + \lambda\tau\left\{\sin\left[(\omega\tau+\vartheta)\frac{\delta}{\tau}\right] - \sin\left[(\omega\tau+\vartheta)\left(1+\frac{\delta}{\tau}\right)\right]\right\}}{\vartheta\cos\left[(\omega\tau+\vartheta)\frac{\delta}{\tau}\right] - \vartheta\cos\left[(\omega\tau+\vartheta)\left(1-\frac{\delta}{\tau}\right)\right] - \lambda\tau\left\{\sin\left[(\omega\tau+\vartheta)\frac{\delta}{\tau}\right] + \sin\left[(\omega\tau+\vartheta)\left(1-\frac{\delta}{\tau}\right)\right]\right\}}, \tag{28}$$

$$K\tau = \frac{[\vartheta^2 + (\lambda\tau)^2]\cos\left[\frac{1}{2}(\omega\tau+\vartheta)\right]}{\lambda\tau\cos\left[\left(\frac{\delta}{\tau}-\frac{1}{2}\right)(\omega\tau+\vartheta)\right] + \vartheta\sin\left[\left(\frac{\delta}{\tau}-\frac{1}{2}\right)(\omega\tau+\vartheta)\right]}. \tag{29}$$

V. BANDPASS FILTERING

In the context of semiconductor lasers, it has been shown both theoretically and experimentally that delayed, bandpass filtered optical feedback is able to suppress the undamping of relaxation oscillations [36,40]. Recently, filtering of an optical feedback signal [41] was also investigated for laser models of Lang-Kobayashi type [42]. In addition, filtered feedback has also been proven important in the investigation of Hopf bifurcation [43], and in the stabilization of unstable periodic orbits by ETDAS in semiconductor superlattices [44]. In order to model this type of modification of the control force, a bandpass filter acting on the feedback force is introduced as a Lorentzian in the frequency domain with the transfer function

$$T(\omega) = \frac{1}{1+i\frac{\omega-\omega_0}{\gamma}}, \tag{30}$$

where ω_0 denotes the peak of the transfer function and γ is half the full width at half maximum of the function. To introduce the filter into the system in the time domain, one can add two additional differential equations to Eq. (1) such that the original two-dimensional system becomes four dimensional:

$$\dot{\mathbf{x}}(t) = \mathbf{A}\mathbf{x}(t) - \mathbf{F}[\bar{\mathbf{x}}(t)],$$

$$\dot{\bar{x}}(t) = \gamma[x(t) - \bar{x}(t)] - \omega_0\bar{y}(t),$$

$$\dot{\bar{y}}(t) = \gamma[y(t) - \bar{y}(t)] + \omega_0\bar{x}(t), \tag{31}$$

where $\bar{x}$ and $\bar{y}$ denote the filtered versions of x and y, respectively. Note that the feedback force $\mathbf{F}[\bar{\mathbf{x}}(t)]$ is now generated from the filtered state vector $\mathbf{x}(t)$ which consists of the two filtered variables $\bar{x}$ and $\bar{y}$:

$$\mathbf{F}[\bar{\mathbf{x}}(t)] = K\sum_{n=0}^{\infty} R^n\{\bar{\mathbf{x}}(t-n\tau) - \bar{\mathbf{x}}[t-(n+1)\tau]\}. \quad (32)$$

Equivalently to the additional differential equations in Eq. (31), the filtering, for instance, in the case of a low pass filter, i.e., $\omega_0=0$, can be expressed by convolution integrals, where the filtered counterparts of $x(t)$ and $y(t)$ are given as follows:

$$\bar{x}(t) = \gamma\int_{-\infty}^{t} x(t')e^{-\gamma(t-t')}dt', \quad (33)$$

$$\bar{y}(t) = \gamma\int_{-\infty}^{t} y(t')e^{-\gamma(t-t')}dt'. \quad (34)$$

The system of differential Eqs. (31) yields a characteristic equation of the form

$$\pm i[\omega_0(\lambda-\Lambda)+\omega(\gamma+\Lambda)] = \gamma K\frac{1-e^{-\Lambda\tau}}{1-\mathrm{Re}^{-\Lambda\tau}} + \omega_0\omega - (\lambda-\Lambda)(\gamma+\Lambda). \quad (35)$$

The minimum feedback gain can be calculated in dependence on ω_0 and γ in similarity to Eq. (11):

$$K_{\min}(\omega_0,\gamma) = \frac{\lambda(1+R)}{2}\left[1+\frac{(\omega_0+\omega)^2+\frac{2\omega_0\omega\lambda}{\gamma}}{(\gamma-\lambda)^2}\right]. \quad (36)$$

Note that at this special value of the feedback gain K, the time delay is no longer given by the intrinsic value $\tau=\pi/\omega$, neither is it the optimal time delay in the general case of nonzero ω_0 and finite values of γ. Adjusting the time delay according to the choice of ω_0 and γ leads to boundaries of the domain of control that can only be understood in the scope of a parametric representation of the boundaries in the (K,R) plane. Such parametric equations can be derived in analogy to Eq. (15). However, the resulting equations for the case of the filtered system are not shown here due to the complexity of the terms.

Figures 12 and 13 depict numerical solutions of the characteristic Eq. (35) for different choices of the parameters γ and ω_0. In Fig. 12 the largest real part of the eigenvalues is shown in dependence on the time delay for different values of the filter width γ in dependence on the time delay. The parameter ω_0 is fixed to 0, which corresponds to the case of a low pass filter. The solid, dashed, dotted, and dash-dotted curves (black, red, green, and blue) correspond to $\gamma T_0=2000$, 40, 10, and 2, respectively. The other control parameters are fixed as $R=0.7$ and $KT_0=0.6$. It can be seen that large values of γ show similar behavior as in the unfiltered system in Fig. 1. Decreasing γ flattens the curves and shifts them up toward positive real parts. Therefore, no control is possible for the case of $\gamma T_0=2$. Additionally, the optimal time delay is shifted to smaller values, which can be seen from the case $\gamma T_0=10$.

In Fig. 13 similar curves are shown for fixed $\gamma T_0=10$ and different choices of the filter's mean value ω_0. The solid, dashed, dotted, and dash-dotted curves (black, red, green, and blue) correspond to $\omega_0 T_0=0$, π, 2π, and 4π, respectively. The other control parameters are fixed as $R=0.7$ and $KT_0=0.6$. It can be observed that the increase of ω_0 shifts the curves further upwards to positive real parts, leading to a less stable system. The range of the time delay for successful control shrinks.

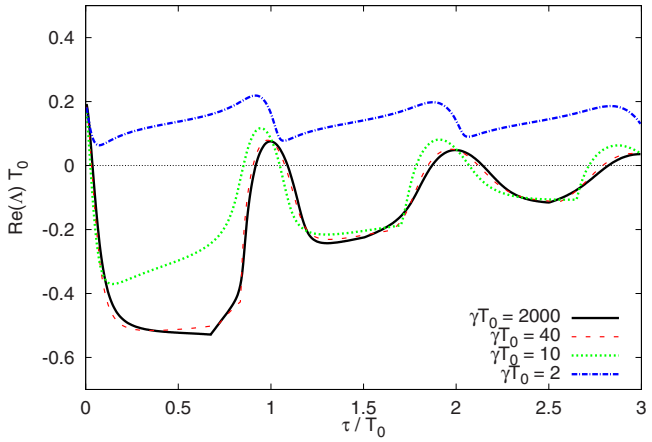

FIG. 12. (Color online) Largest real part of the eigenvalues Λ as a function of τ for different filter widths γ and fixed $\omega_0=0$. The solid, dashed, dotted, and dash-dotted curves (black, red, green, and blue) correspond to $\gamma T_0=2000$, 40, 10, and 2, respectively. The other control parameters are fixed as $R=0.7$ and $KT_0=0.6$. The parameters of the system are as in Fig. 1.

The domain of control can also be investigated in the (K,R) plane. Results are shown in Fig. 14 for different values of the filter width γ and fixed $\omega_0=0$. The black, medium gray, dark gray, and light gray areas (blue, green, red, and yellow) refer to values of $\gamma T_0=2000$, 40, 10, and 2, respectively. The time delay is fixed as $\tau=T_0/2$. The domain of control for large values of γ, here, for instance, $\gamma T_0=2000$

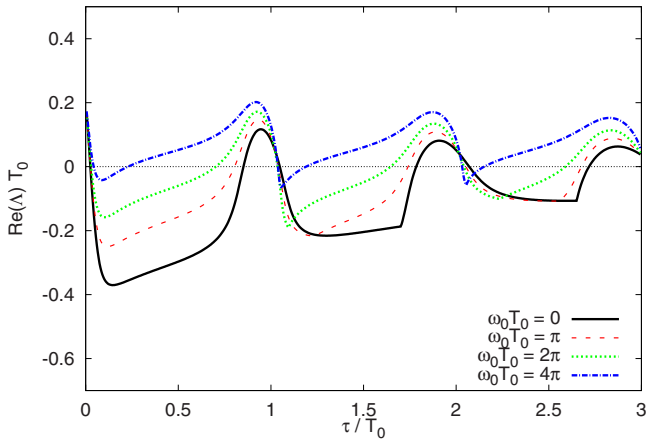

FIG. 13. (Color online) Largest real part of the eigenvalues Λ as a function of τ for different mean values of the filter ω_0 and fixed $\gamma T_0=10$. The solid, dashed, dotted, and dash-dotted curves (black, red, green, and blue) correspond to $\omega_0 T_0=0$, π, 2π, and 4π, respectively. The other control parameters are fixed as $R=0.7$ and $KT_0=0.6$. The parameters of the system are as in Fig. 1.

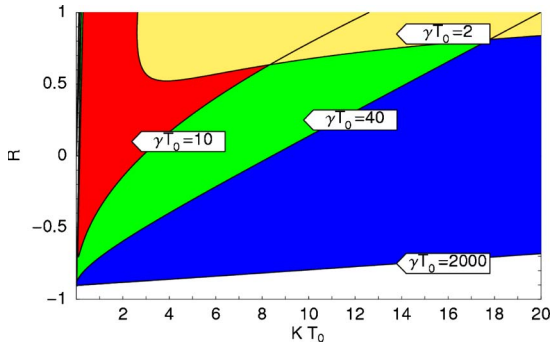

FIG. 14. (Color online) Domain of control in the (K,R) plane for different values of the filter width γ and fixed $\omega_0=0$. The black, medium gray, dark gray, and light gray areas (blue, green, red, and yellow) refer to values of $\gamma T_0=2000$, 40, 10, and 2, respectively. The time delay is fixed as $\tau=T_0/2$. The parameters of the system are as in Fig. 1.

looks very similar to the case of the unfiltered system that is depicted in Fig. 3. Decreasing the value of γ, the region of control shrinks. The lower right boundary is shifted up toward larger values of R. The left boundary, which corresponds to $K_{\min}$ is shifted toward larger values of K. This effect is very small for $\gamma T_0=40$ and 10. For $\gamma T_0=2$, the effect is much more pronounced.

Figure 15 shows the domain of control in the (K,τ) plane for different values of the filter width γ and fixed $\omega_0=0$. Figures 15(a)–15(d) correspond to values of $\gamma T_0=2000$, 40, 10, and 2, respectively, where the time delay is fixed at $\tau=T_0/2$ and $R=0.7$. The case of $\gamma T_0=2000$ looks very similar to the case of the unfiltered system, as shown in Fig. 2. For decreasing value of γ, the tongues shrink in the K direction. The minimum value of K increases and the maximum value becomes smaller. Additionally, the tongues are bent down toward smaller values of the time delay τ with decreasing γ.

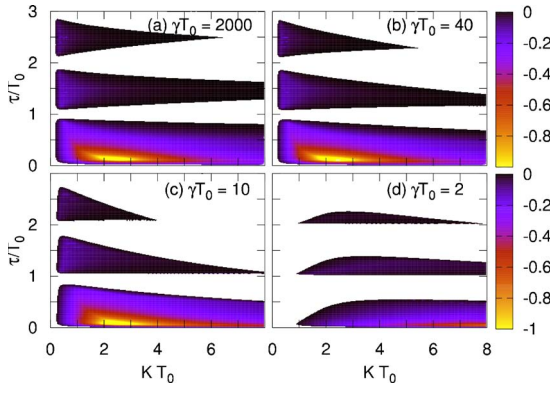

FIG. 15. (Color online) Domain of control in the (K,τ) plane for different values of the filter width γ and fixed $\omega_0=0$. Panels (a), (b), (c), and (d) correspond to values of $\gamma T_0=2000$, 40, 10, and 2, respectively, where the time delay is fixed at $\tau=T_0/2$ and $R=0.7$. The grayscale (color code) shows the largest real part of the complex eigenvalues Λ as given by Eq. (35). Only negative values are displayed. The parameters of the system are as in Fig. 1.

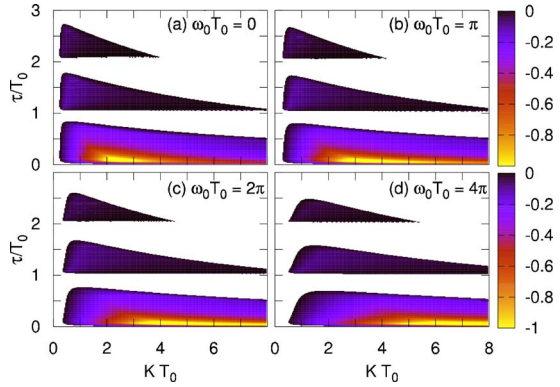

FIG. 16. (Color online) Domain of control in the (K,τ) plane for different values of the filter's mean value ω_0 and fixed $\gamma T_0=10$. Panels (a), (b), (c), and (d) correspond to values of $\omega_0 T_0=0$, π, 2π, and 4π, respectively, where the time delay is fixed at $\tau=T_0/2$ and $R=0.7$. The grayscale (color code) shows the largest real part of the complex eigenvalues Λ as given by Eq. (35). Only negative values are displayed. The parameters of the system are as in Fig. 1.

This leads to an optimal τ that is smaller than in the unfiltered case.

In Fig. 16 the filter width is fixed to $\gamma T_0=10$, the domain of control is shown for different values of the filter's mean values ω_0. Figures 16(a)–16(d) correspond to values of $\omega_0 T_0=0$, π, 2π, and 4π, respectively, where the time delay is fixed at $\tau=T_0/2$ and $R=0.7$. The size of the domain of control is only slightly changed with increasing ω_0. The domains are flattened on the upper side for larger values of ω_0. The region of optimal control, denoted by bright (yellow) color, is additionally shifted slightly toward larger values of the feedback gain K and shrinks in the τ direction. Overall, the variation of ω_0 has very little effect on the domain of control in the (K,τ) plane.

VI. CONCLUSION

In conclusion, we have shown that extended time-delayed feedback can be used to stabilize unstable steady states of focus type. By introduction of an additional memory parameter, this method is able to control a larger range of unstable fixed points compared to the original TDAS scheme. However, the degree of stability, measured by the absolute value of the real part of the eigenvalue, is generally decreased. We have investigated the domain of control in various one- and two-dimensional projections of the space spanned by the control parameters. Furthermore, we have also discussed effects of nondiagonal coupling, nonzero control loop latency, and bandpass filtering of the control signal, which are relevant in an experimental realization of the ETDAS control method. We found that a proper adjustment of the time delay is able to compensate for reducing stabilization abilities of the control method, for instance, due to latency or feedback

phase. We point out that the results obtained in this paper are accessible for applications in the context of all-optical control of intensity oscillations of semiconductor lasers as investigated in Ref. [37].

ACKNOWLEDGMENT

This work was supported by Deutsche Forschungsgemeinschaft in the framework of Sfb 555.

[1] E. Ott, C. Grebogi, and J. A. Yorke, Phys. Rev. Lett. **64**, 1196 (1990).
[2] N. Baba, A. Amann, E. Schöll, and W. Just, Phys. Rev. Lett. **89**, 074101 (2002).
[3] *Handbook of Chaos Control*, edited by E. Schöll and H. G. Schuster, second completely revised and enlarged edition (Wiley-VCH, Weinheim, 2007).
[4] K. Pyragas, Phys. Lett. A **170**, 421 (1992).
[5] A. G. Balanov, N. B. Janson, and E. Schöll, Phys. Rev. E **71**, 016222 (2005).
[6] A. Ahlborn and U. Parlitz, Phys. Rev. Lett. **93**, 264101 (2004).
[7] M. G. Rosenblum and A. S. Pikovsky, Phys. Rev. Lett. **92**, 114102 (2004).
[8] P. Hövel and E. Schöll, Phys. Rev. E **72**, 046203 (2005).
[9] J. E. S. Socolar, D. W. Sukow, and D. J. Gauthier, Phys. Rev. E **50**, 3245 (1994).
[10] M. E. Bleich and J. E. S. Socolar, Phys. Lett. A **210**, 87 (1996).
[11] W. Just, T. Bernard, M. Ostheimer, E. Reibold, and H. Benner, Phys. Rev. Lett. **78**, 203 (1997).
[12] W. Just, D. Reckwerth, J. Möckel, E. Reibold, and H. Benner, Phys. Rev. Lett. **81**, 562 (1998).
[13] K. Pyragas, Phys. Rev. Lett. **86**, 2265 (2001).
[14] S. Yanchuk, M. Wolfrum, P. Hövel, and E. Schöll, Phys. Rev. E **74**, 026201 (2006).
[15] H. Nakajima, Phys. Lett. A **232**, 207 (1997).
[16] B. Fiedler, V. Flunkert, M. Georgi, P. Hövel, and E. Schöll, Phys. Rev. Lett. **98**, 114101 (2007).
[17] W. Just, S. Popovich, A. Amann, N. Baba, and E. Schöll, Phys. Rev. E **67**, 026222 (2003).
[18] W. Just, H. Benner, and C. v. Löwenich, Physica D **199**, 33 (2004).
[19] D. J. Gauthier, Opt. Lett. **23**, 703 (1998).
[20] K. Pyragas, Phys. Lett. A **206**, 323 (1995).
[21] K. Pyragas, Phys. Rev. E **66**, 026207 (2002).
[22] O. Beck, A. Amann, E. Schöll, J. E. S. Socolar, and W. Just, Phys. Rev. E **66**, 016213 (2002).
[23] J. Unkelbach, A. Amann, W. Just, and E. Schöll, Phys. Rev. E **68**, 026204 (2003).
[24] P. Hövel and J. E. S. Socolar, Phys. Rev. E **68**, 036206 (2003).
[25] J. Pomplun, A. Balanov, and E. Schöll, Phys. Rev. E **75**, 040101(R) (2007).
[26] E. M. Wright, Proc. R. Soc. Edinburgh, Sect. A: Math. Phys. Sci. **62**, 387 (1949).
[27] J. K. Hale, in *Functional Differential Equations,* Vol. 3 of *Applied Mathematical Sciences* (Springer, New York, 1971).
[28] A. Amann, E. Schöll, and W. Just, Physica A **373**, 191 (2007).
[29] W. Just, E. Reibold, H. Benner, K. Kacperski, P. Fronczak, and J. Holyst, Phys. Lett. A **254**, 158 (1999).
[30] S. Bielawski, M. Bouazaoui, D. Derozier, and P. Glorieux, Phys. Rev. A **47**, 3276 (1993).
[31] D. Pieroux, T. Erneux, and K. Otsuka, Phys. Rev. A **50**, 1822 (1994).
[32] O. Ushakov, S. Bauer, O. Brox, H. J. Wünsche, and F. Henneberger, Phys. Rev. Lett. **92**, 043902 (2004).
[33] S. Bauer, O. Brox, J. Kreissl, B. Sartorius, M. Radziunas, J. Sieber, H. J. Wünsche, and F. Henneberger, Phys. Rev. E **69**, 016206 (2004).
[34] V. Z. Tronciu, H. J. Wünsche, M. Wolfrum, and M. Radziunas, Phys. Rev. E **73**, 046205 (2006).
[35] A. Gavrielides, T. Erneux, D. W. Sukow, G. Burner, T. McLachlan, J. Miller, and J. Amonette, Opt. Lett. **31**, 2006 (2006).
[36] A. Fischer, O. Andersen, M. Yousefi, S. Stolte, and D. Lenstra, IEEE J. Quantum Electron. **36**, 375 (2000).
[37] S. Schikora, P. Hövel, H. J. Wünsche, E. Schöll, and F. Henneberger, Phys. Rev. Lett. **97**, 213902 (2006).
[38] M. G. Rosenblum and A. Pikovsky, Phys. Rev. E **70**, 041904 (2004).
[39] H. Nakajima and Y. Ueda, Physica D. **111**, 143 (1998).
[40] M. Yousefi and D. Lenstra, IEEE J. Quantum Electron. **35**, 970 (1999).
[41] H. Erzgräber, B. Krauskopf, D. Lenstra, A. P. A. Fischer, and G. Vemuri, Phys. Rev. E **73**, 055201(R) (2006).
[42] R. Lang and K. Kobayashi, IEEE J. Quantum Electron. **16**, 347 (1980).
[43] L. Illing and D. J. Gauthier, Physica D **210**, 180 (2005).
[44] J. Schlesner, A. Amann, N. B. Janson, W. Just, and E. Schöll, Phys. Rev. E **68**, 066208 (2003).